

A wirelessly powered and controlled device for optical neural control of freely-behaving animals

Christian T Wentz^{1,2,3}, Jacob G Bernstein^{2,3}, Patrick Monahan^{2,3},
Alexander Guerra^{2,3}, Alex Rodriguez^{2,3} and Edward S Boyden^{2,3,4,5,6}

¹ Department of Electrical Engineering and Computer Science, Massachusetts Institute of Technology, 77 Massachusetts Ave, Cambridge, MA 02139, USA

² McGovern Institute for Brain Research, Massachusetts Institute of Technology, 77 Massachusetts Ave, Cambridge, MA 02139, USA

³ Media Lab, Massachusetts Institute of Technology, 77 Massachusetts Ave, Cambridge, MA 02139, USA

⁴ Department of Brain and Cognitive Sciences, Massachusetts Institute of Technology, 77 Massachusetts Ave, Cambridge, MA 02139, USA

⁵ Department of Biological Engineering, Massachusetts Institute of Technology, 77 Massachusetts Ave, Cambridge, MA 02139, USA

E-mail: esb@media.mit.edu

Received 28 January 2011


Accepted for publication 19 May 2011

Published 23 June 2011

Online at stacks.iop.org/JNE/8/046021

Abstract

Optogenetics, the ability to use light to activate and silence specific neuron types within neural networks *in vivo* and *in vitro*, is revolutionizing neuroscientists' capacity to understand how defined neural circuit elements contribute to normal and pathological brain functions. Typically, awake behaving experiments are conducted by inserting an optical fiber into the brain, tethered to a remote laser, or by utilizing an implanted light-emitting diode (LED), tethered to a remote power source. A fully wireless system would enable chronic or longitudinal experiments where long duration tethering is impractical, and would also support high-throughput experimentation. However, the high power requirements of light sources (LEDs, lasers), especially in the context of the extended illumination periods often desired in experiments, precludes battery-powered approaches from being widely applicable. We have developed a headborne device weighing 2 g capable of wirelessly receiving power using a resonant RF power link and storing the energy in an adaptive supercapacitor circuit, which can algorithmically control one or more headborne LEDs via a microcontroller. The device can deliver approximately 2 W of power to the LEDs in steady state, and 4.3 W in bursts. We also present an optional radio transceiver module (1 g) which, when added to the base headborne device, enables real-time updating of light delivery protocols; dozens of devices can be controlled simultaneously from one computer. We demonstrate use of the technology to wirelessly drive cortical control of movement in mice. These devices may serve as prototypes for clinical ultra-precise neural prosthetics that use light as the modality of biological control.

 Online supplementary data available from stacks.iop.org/JNE/8/046021/mmedia

⁶ Author to whom any correspondence should be addressed.

1. Introduction

Technologies for using light to activate and silence specific cell types in the brain of the behaving animal are revolutionizing neuroscientists' capacity to understand how defined neural circuit elements contribute to normal and pathological brain functions. In such experiments, viral or transgenic approaches are used to deliver genes that encode light-gated ion transport proteins, such as ChR2, Halo/NpHR, Arch, Mac and others, to specific cells, pathways, or regions in the brain [1–5]. In order to deliver light to the neural circuit *in vivo*, typically experimenters insert an optical fiber into the brain, tethered to a remote laser [6, 7], or implant a light-emitting diode (LED) over the top of the brain, tethered to a remote power source [8]. However, tethered experimental setups present several problems for the experimenter. Animals must be handled at the beginning of each experiment, which can alter behavior. Tethering may be impractical for optogenetic experiments over long periods of time such as desired in many developmental, longitudinal, disease-progression, or other chronic-perturbation experiments, where fibers and cables risk breakage or binding over time. Finally, the need for tethering sets limits on the number of animals that can be manipulated in a single experiment (e.g. a social experiment with multiple mice could result in tangling or breakage of the tethers) or in parallel experiments (e.g. in high-throughput screening of large sets of animals). Ideally, for such experiments a fully wireless system would be available, enabling chronic and longitudinal experiments, and supporting experimentation with large numbers of animals. Wireless electrical stimulation and optical modulation approaches have already been demonstrated utilizing batteries for energy storage [9, 10]. While certainly useful in many applications, battery-based systems suffer from a limited operational time between charges and, particularly with the high current requirements of LED light sources, may be prohibitively large for rodent experiments when many LEDs are required, or when high current LEDs are utilized (e.g. for targeting of deep brain structures). The ability to update modulation protocols in real time to suit behavior-dependent paradigms or other complex experimental paradigms would also be of great use.

In order to satisfy the power and control requirements for freely-behaving optogenetic experiments, we have developed a supercapacitor-based headborne device which can control multiple headborne LEDs, receiving power (and optionally, real-time delivered stimulation protocol information) in a fully wireless fashion. The device is small ($<1\text{ cm}^3$), and weighs approximately 2 g when operated autonomously with pre-programmed modulation protocols, or 3 g when equipped with optional wireless telemetry, both implementations being appropriate for use in small animals such as mice. In this paper we present the design, which centers around a high-efficiency resonant wireless power transfer system and headborne supercapacitor-based energy storage, appropriate to support the reliability and high-power operation requirements of the optogenetic research. The power transmitters are low-profile devices that can fit under behavioral arenas or cages. We show that such systems can sustain multi-watt power delivery

both continuously and in burst mode, and demonstrate control of behavior in untethered mice expressing ChR2 in motor cortex pyramidal cells. Such systems will not only enable a number of fundamentally new kinds of experiment, but may also serve as prototypes for a new generation of clinical neural prosthetics that achieve great precision through the use of light-targetable molecules as the transducers of cell-type-specific neural control.

2. Materials and methods

2.1. Design and fabrication

The complete wireless optical neural control system consists of a headborne device (depicted in figure 1), a wireless power transmitter (depicted in figure 2(a)) and a USB-connected wireless base station (shown in figure 2(b)) for communication with the headborne device. We describe here the design and fabrication of these elements.

2.1.1. Headborne device. The headborne device comprises four distinct modules—the power, radio, motherboard and optics modules. The optics module, containing the LED light sources, is surgically affixed to the skull, while the remainder of the device (the motherboard module, the power module, and the optional radio module) is attached to the optics module via a low insertion force connector (figure 1(f)).

Unless otherwise noted, construction of modules is as follows: circuit schematics for the power, radio, motherboard, and optics modules (see supplementary files available at stacks.iop.org/JNE/8/046021/mmedia) are created using Eagle CAD Professional (Cadsoft). The radio and motherboard modules are designed as four-layer printed circuit boards (PCBs) using Eagle CAD Professional and fabricated by Advanced Circuits. PCBs are populated with parts (see supplementary files available at stacks.iop.org/JNE/8/046021/mmedia) using standard solder paste and reflow oven techniques.

As identified in the board-level drawings (figure 1(b)) and module photographs (figure 1(c)), the radio module shown at top contains a surface mount antenna (1; note: numbers here refer to the flagged items in figures 1(a)–(c)), a 1 Mbit s⁻¹ radio chipset operating in the ISM 2.4–2.485 GHz band (2), and a six-pin radio-to-motherboard docking connector (3). Calculated matching network component values for the radio module were verified in simulation using LT Spice IV/SwitcherCAD III (Linear Technology).

The power module (shown second from top in figures 1(b) and (c)) consists of a receiver element for power reception (4), a full-wave rectifier for ac to dc conversion (5), a supercapacitor (6) and a power-to-motherboard docking connector (7). Calculated passive component values for the power module tank circuit were simulated using LT Spice IV/SwitcherCAD III. To minimize device size, the power module is assembled without a PCB, instead using the body of the supercapacitor as a structural element onto which all the parts are mounted using epoxy. The male power connector is used as a structural element to affix the power receiver antenna.

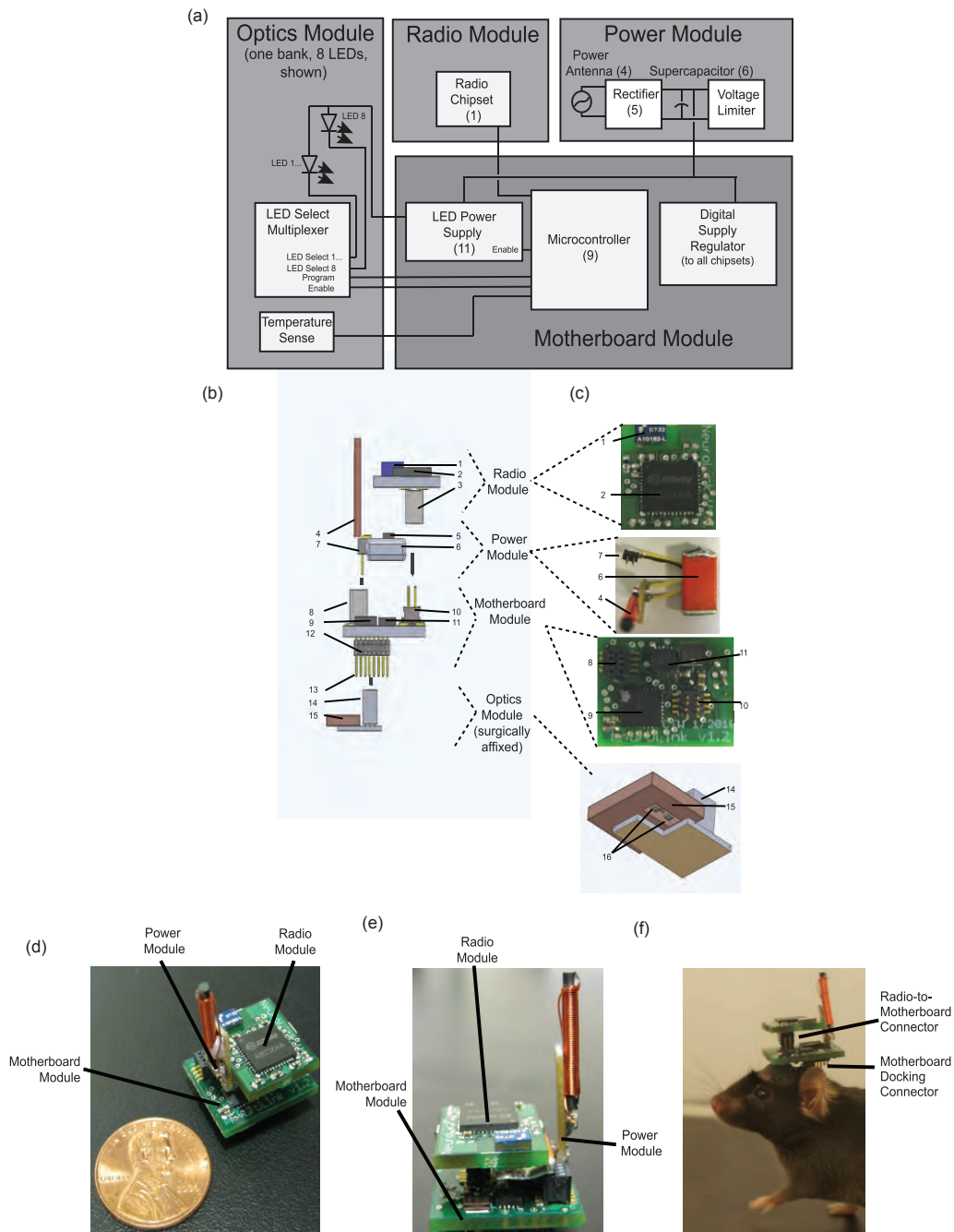


Figure 1. Design and implementation of a wirelessly powered and controlled headborne optical neural control device. (a) Block diagram of the device, which comprises three core modules (power, which contains the supercapacitor and antenna, optics, which holds up to 16 LEDs in two banks of eight each; motherboard, which contains the microcontroller and power circuitry), as well as one optional module (radio module, which mediates on-line updating from a computer or laptop). (b) Schematic side view and (c) three-dimensional representations of the modules that make up the device, with numbers indicating some of the key parts used. The optional radio module contains an antenna (1), a radio chipset (2), and a motherboard-docking connector (3). The power module contains an antenna for power reception (4), a power rectifier chip (5), a supercapacitor (6), and a motherboard-docking connector (7). The motherboard module contains a microcontroller (9), an LED power supply (11), and connectors for docking the power (8), radio (10), and optics modules (12); the ten pins on connector 12 that are not used by the optics module are used for post-device assembly programming of the microcontroller (e.g. as seen in figure 2(b), which shows a motherboard + radio connected to a laptop through a USB-connected base station board (the red board) in the fashion required for reprogramming). The optics module, which is cemented to implanted skull screws and acts as the support for the detachable three remaining components of the device, comprises a connector that docks to the motherboard module (14), a copper thermal sink that also serves as an isolated ground for the LEDs (15), one or more LEDs (16) and a temperature sensor (not shown, mounted on bottom of the copper post-machining of thermal sink; see supplementary files available at stacks.iop.org/JNE/8/046021/mmedia for schematic), as well as the LED multiplexer (attached to the side of the connector; see supplementary files available at stacks.iop.org/JNE/8/046021/mmedia). (d) Angled and (e) side view of the detachable portion of the device (radio, power, motherboard; optics module is not shown), with penny shown for scale. (f) Headborne electronics unit affixed to the subject via a low insertion force connector between the optics module (surgically affixed) and the motherboard module. Supercapacitor removed to show connector interfaces between the motherboard and radio modules.

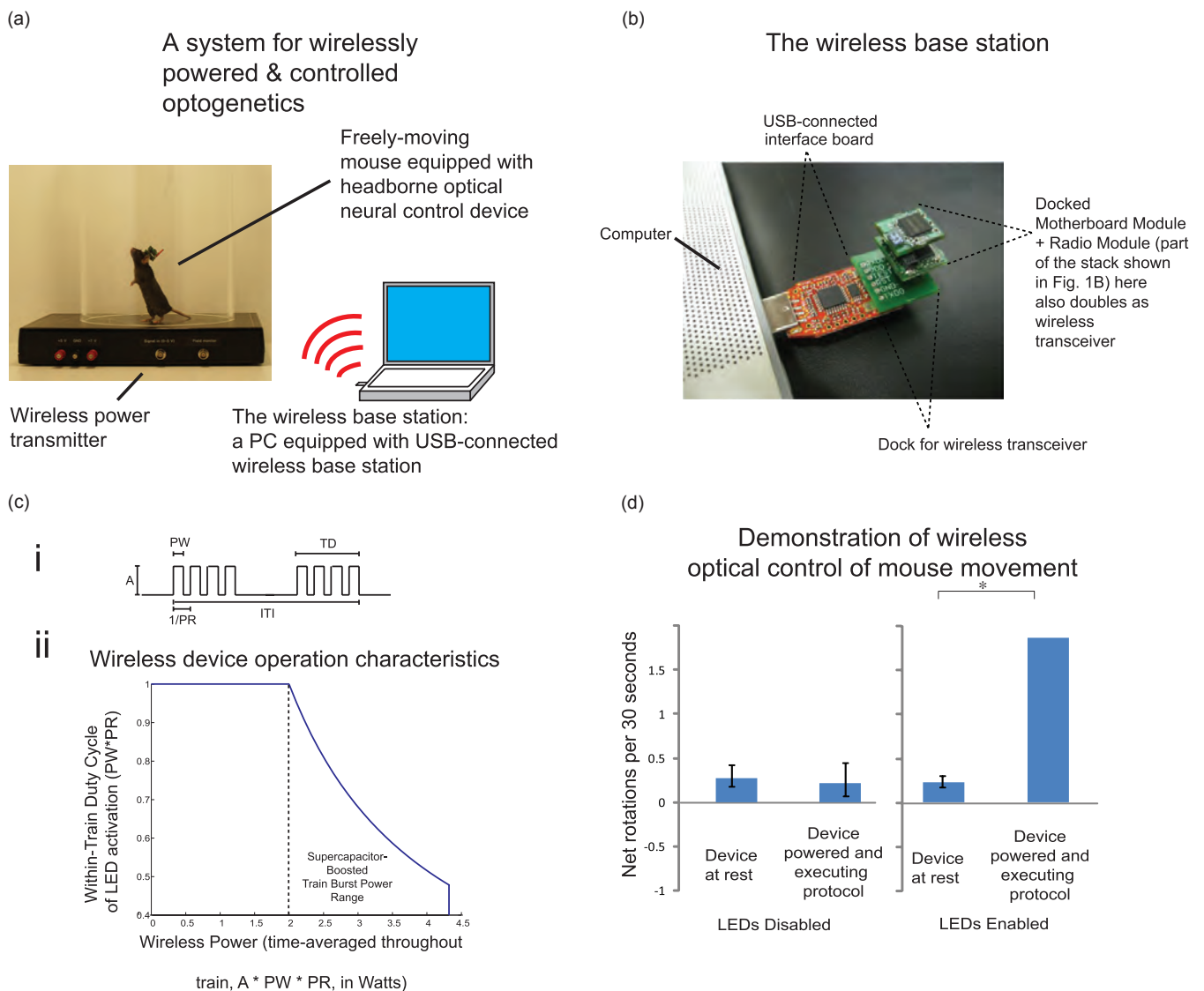


Figure 2. A simple wireless power and communication interface for operation of headborne optical neural control devices on the awake behaving mouse. (a) Photograph of an arena equipped with a power transmitter coil (a 120 kHz LC tank circuit), containing a mouse equipped with a headborne optical neural control device; schematic showing operation with a computer, base station attached via a USB port (detailed photograph of the base station in (b)). When powered up, the microcontroller automatically initializes the radio module if attached, wirelessly connecting to the base station to receive instruction from the experimenter; if no radio module is attached, can operate in open-loop fashion. (b) Photograph of a USB-connected wireless interface board (red) docked to a laptop, and equipped with a copy of a headborne device (green) to serve as the transceiver for wireless communication (collectively denoted the base station). (c) Guidelines for usage of wireless headborne optical control devices for typical neuroscience experiments involving pulse trains of light delivery. (i) We introduce a schema defining various properties of pulse trains (i.e. within-train duty cycle = $PW/(1/PR)$, and within-train average power = $A \cdot PW/(1/PR)$), for assistance with visualizing typical protocols for device operation. (ii) Plot of the range of typical protocols for device operation, expressed as a function of within-train duty cycle and within-train average power, assuming that the between-train pause (i.e. $ITI - 2 \cdot TD$) is at least 3 s. Any point under the curve is easily achievable. Because the power antenna continuously receives 2 W, the device can run indefinitely with a time-averaged power of 2 W; the device can exceed 2 W using the supercapacitor's excess capacity, but with reduced duty cycle, and never crossing the device maximum peak power of 4.3 W. In addition, there is no hit in device performance with between-train pauses of less than 3 s if 2 W or less is consumed; if more than 2 W is consumed, because the supercapacitor's excess capacity is needed, some time (up to 3 s, depending on how much energy is used) will be required to recharge the supercapacitor in between the LED-on periods that drain the supercapacitor. (d) Unilateral optogenetic control of motor cortex neurons in a freely behaving Thy1-ChR2 mouse, which expresses ChR2 in layer 5 pyramidal cells (right), eliciting reliable drive of mouse rotation compared to the no-light condition before stimulation ($n = 9$ trials across two subjects, positive value indicates CCW rotation, * indicates $p < 0.01$, paired t -test). When the LEDs were turned off (left), no rotation was apparent ($p > 0.5$, $n = 5$ trials, paired t -test).

A wiring harness connects the supercapacitor assembly to the connector/antenna assembly. The power receiver element of the RF link consists of a resonant parallel LC tank circuit, built of a 15 mm long, 2 mm diameter wound copper ferrite core

and a ceramic tuning capacitor with a resonant frequency of 120 kHz.

The motherboard module, shown second from bottom in figures 1(b) and (c), contains the microcontroller (9), two-stage

LED power conditioning circuitry (11), and connectors for docking the power (8), radio (10), and optics modules (12); the ten pins on connector 12 that are not used by the optics module are used for programming of the microcontroller (e.g. as seen in figure 2(b), which shows a motherboard + radio connected to a laptop through the USB-connected interface board (red board). Note well that figure 2(b) shows a USB-connected interface board with a copy of the motherboard + radio module docked to it; when such a copy of the motherboard + radio module is docked to the interface board, this docked pair of modules serves as a transceiver to communicate with one or more headborne devices in an experiment (see below). When assembled as shown in figure 2(b), the device is referred to as the wireless base station.

Programs running on the motherboard's microcontroller (in supplementary files available at stacks.iop.org/JNE/8/046021/mmedia) were written in C using the IAR Embedded Workbench development environment (IAR Systems). Radio communication protocols were built on top of the SimpliciTI network protocol developed by Texas Instruments. Compiled programs were downloaded to the microcontroller on the motherboard module using the USB-connected interface board, as described in the previous paragraph. The interface board comprises a microcontroller development tool (Texas Instruments EZ430-RF2500) that we modified with a custom docking circuit board so as to interface the EZ430 USB tool to the motherboard module.

The optics module, shown at bottom in figures 1(b) and (c), comprises a connector that docks to the motherboard module (14), a copper thermal sink that acts as a structure to mate bare die LEDs (16) up to 1 mm × 1 mm in size each, and also serves as a cathode for LEDs (15), and a thermistor acting as temperature sensor (mounted on bottom of the copper; see supplementary files available at stacks.iop.org/JNE/8/046021/mmedia for schematic), as well as the LED multiplexer (attached to the side of the connector; see supplementary files available at stacks.iop.org/JNE/8/046021/mmedia). A custom PCB milled from gold plated FR4 board stock acts as a common structural element to link the copper sink containing LEDs, the optics-to-motherboard mating connector and integrated circuitry. The optics module PCB schematic and layout was designed using Eagle CAD Professional, and then exported using a custom Python script to be machined by a three-axis tabletop milling machine (Modella). The copper thermal block was machined with a waterjet cutter (Omax) from copper bar stock and the underside LED mounting surfaces were then milled out using the tabletop mill. In this instantiation of the device, 1 mm × 1 mm bare die LEDs (16) were reflow soldered to milled out pedestals in the copper, and the resulting LED + thermal block assembly was reflow soldered to the top side of the PCB. Finally, anodic electrical connections from individual LEDs to PCB traces were made using aluminum wedge wire bonds (0.001" diameter). For robustness, bare die wire-bonded LEDs were coated with a protective layer of UV cured clear optics glue (Thorlabs) and the remainder of the underside of the device was potted in black epoxy to ensure electrical isolation from tissue. Following these assembly

steps, a miniature 0201-sized thermistor is epoxied to the copper thermal block using thermally conductive epoxy for temperature monitoring via the microcontroller.

2.1.2. Wireless power transmitter. Power is coupled wirelessly from an under-arena power transmitter (Ferro Solutions) to the headborne device using resonant energy transfer over distances of several centimeters using a low-strength oscillating magnetic field (peak 300 A m⁻¹), as diagrammed in figure 2(a). (For a plot of the magnetic field, M , versus vertical distance above the transmitter, see supplementary figure 5 available at stacks.iop.org/JNE/8/046021/mmedia.) The arenas used in our prototyping and experiments were either a circular mouse cage or a circular bowl of ~8" in diameter. The under-cage power transmitter consists of a resonant series LC circuit tuned to the frequency of the power receiver circuit (in this instantiation 120 kHz) and an asynchronous bridge driver to drive the LC circuit at this frequency, as described previously in [11].

In this instantiation of our system, the under-cage power transmitter was powered from an external dual channel power supply (Agilent E3646A); separate power supplies serve the LC circuit and the bridge driver control circuitry. A control signal to the bridge driver was supplied externally via a programmable function generator (Stanford Research Systems DS345) connected via 50 Ω terminated BNC cable. Thus, the receiver element of the headborne device is orthogonal to the floor of the cage, seen in figures 1 and 2(a), such that it maximally couples the transmitter's oscillating magnetic field.

2.1.3. USB-connected base station. The USB-connected base station serves two functions: (1) to program the assembled headborne electronics unit before attaching to the animal (as described above), and (2) to wirelessly communicate with headborne devices. The USB-connected base station consists of an interface board (figure 2(b), red—Texas Instruments), a custom docking board, a motherboard module and a radio module identical to those used in the headborne devices. When equipped with a copy of the headborne device to serve as a radio transceiver (comprising the base station), the microcontroller provides a seamless wireless communication interface between headborne devices on animal subjects and the PC to which the base station is attached.

2.2. Animal preparation and experimental setup

Adult Thy-1-ChR2 transgenic mice (eight–ten weeks old, ~30 g, line 18 in [12, 13]) were utilized in this experiment. All animal procedures and protocols were approved by the MIT Committee on Animal Care.

2.2.1. Surgery and animal preparation. Mice were anesthetized using 1.5% isoflurane in oxygen. The top of the head was shaved and the animal was placed in a stereotax (Kopf). Betadine and 70% ethanol was used to sterilize the surgical area and ophthalmic ointment was applied to the eyes.

A mid-line scalp incision was made, and the skin retracted. At a center point of anterior–posterior (AP) 2.0, medio-lateral (ML) 2.0 relative to bregma, the skull thickness was thinned using a dental drill to create a 2 mm × 2 mm bone window for the LED implant to sit in. Three surgical screws were inserted into the skull to secure the implant. Kwik-Sil (World Precision Instruments) silicone elastomer was used to fix the implant in place temporarily, and to improve the light transmission efficiency between the LED and brain tissue. Dental acrylic (Stoelting) was then used to affix the implant to the screws and the skull. The animals were allowed to recover for five days prior to behavioral testing.

One LED was targeted unilaterally to M1 motor cortex (AP −1.0 mm, ML 0.5 mm). An additional LED was included for debugging purposes, targeted to M2 cortex (AP −0.3 mm, ML 0.5 mm), but not used in the experiment.

2.2.2. Motor control experimental setup. Mice were acclimated with headborne devices for at least 15 min prior to behavioral testing in the experiment arena consisting of a plastic bowl (approximately 8" diameter) with an under-cage power transmitter operating at 5 A. A CCD camera (Logitech) was suspended above the arena to record behavior. We delivered LED illumination to M1 cortex (15 ms pulse width, 30 Hz) at 250 mW input power to the LED for 30 s followed by 90 s off time, repeated four–five times in a session. After the experiment, animal rotation was scored in 30 s epochs before and during the illumination phase. Rotation was scored as the number of net rotations within the 30 s epoch to the nearest quarter rotation (positive rotations being counter-clockwise), and is plotted in figure 2(d). An additional control experiment was performed, in which identical power levels and control signals were transmitted, but with LEDs disabled via the LED controller chipset. Thus, in this control experiment subjects are exposed to identical electrical and magnetic fields, but are not driven optically. Statistical analyses were performed in Excel (Microsoft).

2.2.3. Measurement of the emitted magnetic field. To quantify the magnetic field produced by the wireless power transmitter, we applied a dc current to the transmitter coil (5 A), identical in magnitude to that used in normal operation, and measured the resulting magnetic field, M , at varying heights above the center of the transmitter coil, where field strength is maximal, using a Lakeshore 450 Gauss meter. A plot of the resulting magnetic field profile is shown in supplementary figure 4 available at stacks.iop.org/JNE/8/046021/mmedia.

2.2.4. Bench measurement of optics module temperature. To measure optics module temperature, we utilized a K-type thermocouple (Omega Engineering) affixed to the tissue interface side of a non-implanted optics module at room temperature and cycled power to the LED via the headborne electronics unit using parameters identical to those in our motor control experiments (30 Hz, 15 ms duty cycle, and 250 mW input power to the LED). The

resulting temperature of the tissue interface side of the optics module was measured using a calibrated Omega HH506RA data logger (plotted in supplementary figure 5 available at stacks.iop.org/JNE/8/046021/mmedia).

3. Results

3.1. Device description and rationale for design

We set out to develop a compact, robust optogenetic neural control device that is capable of supporting experiments in which use of untethered freely-behaving animals is desired. In this section, we describe the design of the system and principles of operation. In the following section we describe actual use of the wireless optogenetic tool in an experimental paradigm.

To achieve the functionality desired for freely-behaving optogenetic experiments, we developed a modular headborne electronic device (figure 1), accompanied by a wireless power transmitter which resides underneath the behavioral arena (e.g. cage or maze), and a USB-connected base station to enable wireless control of headborne devices using a standard computer (figure 2). The headborne device consists of four different modules, namely the optics, motherboard, power and radio modules, which dock together to provide, respectively, the light delivery, waveform generation, power receiving and communication functions necessary to achieve untethered optogenetic control. Light delivery to target tissue is achieved via an optics module (figures 1(b) and (c), shown at the bottom) that contains a number of LEDs mounted in a compact structure that provides both electrical power delivery to the LEDs and dissipation of heat generated during their operation. In the current embodiment, the optics module can hold up to 16 LEDs, which are individually controllable via an on-module multiplexing circuit that is operated by digital signals from a microcontroller residing on the motherboard module. The optics module is the only part of the headborne device that is chronically implanted on the mouse skull; the other three modules dock together into an electronics stack that plugs into the optics module, either after the surgery is complete or before the experiment is about to begin. The microcontroller that controls the optics module is located on the motherboard module (figures 1(b) and (c), second from bottom), which serves not only as the core structural element of the electronics stack, but also helps the device achieve efficient wireless power by actively regulating the LED power circuitry and the transfer of energy, received wirelessly via resonant power transfer, to a storage supercapacitor. To facilitate real-time updating of control waveforms, the microcontroller can also receive radioed instructions via the optional radio module (figures 1(b) and (c), top), which docks to the motherboard module, and communicates with a base station equipped remote PC (figure 2(b)). To wirelessly receive and store power for device operation, the power module contains both a resonant wireless energy receiver as well as a storage supercapacitor, and docks to the motherboard module (figures 1(b) and (c), second from top).

The modular headborne device described above is depicted in block diagram fashion in figure 1(a), each

module being represented by a gray box, and with the major subcomponents enabling the functionality of each of the optics (left), radio (top-center), power (top-left), and motherboard (bottom-right) modules shown in white boxes. Black traces crossing between each gray box represent the major control and power interconnects between modules. As can be seen in figure 1(b), the power and control interconnects are made using small form factor low insertion force connectors (Samtec), allowing their disassembly, but ensuring the device remains connected during a long-term experiment. The complete electronics stack consisting of radio, power and motherboard modules seen in figure 1(c) is shown as a unit in figures 1(d) and (e), and affixed to a subject in figure 1(f) (supercapacitor removed to show connector interfaces).

Each of these modules was designed with a set of strategies in mind to achieve three core goals: (i) high power density to support operation of several LEDs, (ii) flexible and simple device operation in a variety of experiment protocols and (iii) robust, reliable operation. Throughout all modules, compactness, robustness and flexibility were achieved by using off-the-shelf parts, chip-scale packaging and highly integrated system-on-chip circuit components wherever available. The modularity of the physical device layout, with easily replaceable subsystems, allows for rapid incremental improvement of the design. Specific modules were further optimized to meet the above goals as described below.

The central strategy that enables this system to achieve high power density is the use of a supercapacitor-based power module to store and buffer wirelessly received power. By utilizing a supercapacitor energy storage element and wireless recharging approach rather than battery-based implementation, this device is able to achieve a greater than $10\times$ reduction in size over other battery-based approaches, while increasing the maximum peak power deliverable to LEDs by approximately $15\times$ over previous designs [14], and allowing the system to operate at these power levels indefinitely. The reason for such substantial size reduction with increased power delivery over previous battery-based approaches lies in the physical constraints: although batteries are capable of high energy density, they achieve power densities several orders of magnitude lower than those of supercapacitors [15]. This is a critical observation because optics systems utilizing LEDs to drive pulsatile or enduring illumination protocols, as is commonly desired in optogenetic experiments, have high-power requirements but only modest energy requirements (that is, the peak-to-average power ratio is high, due to the low duty cycle of most optogenetic experiments). Most batteries are able to supply a discharge current rating of $1-5C^{-1}$ (where C is the total energy capacity of the battery). Because the peak power requirement of an LED-based system is quite high (approximately 400 mA @ 3.6 V per LED with 1 mm \times 1 mm LEDs), but the time-averaged power of a pulse train may be more modest, the peak power discharge rate limitation of the battery-based solution necessitates use of a battery much larger than needed based on the energy requirements of the system. Thus, by utilizing a constant wireless energy transfer link operating at the time-averaged power of the system (which may be at a lower level

than the peak power utilized by the LEDs), the supercapacitor provides an energy buffer to deliver bursts of pulse trains at multi-watt levels, without needing to store on the animal any of the unused energy capacity required for the battery-based approach. Operating the device at matched resonant frequencies with a high Q (>100) receiver circuit maximizes wirelessly coupled energy transfer efficiency [15].

The flexibility and simplicity of use is achieved through the software reconfigurability of the headborne device. To enable many different types of experiments to be performed, the motherboard module can be programmed to generate multiple independent waveforms, either running continuously in pre-programmed fashion or triggered and updated remotely by commands via the wireless communication link (e.g. based on a behavioral input to the computer such as a nose poke or other cue, or manually triggered). Multiplexers residing on the optics module and controlled by commands from the motherboard module (or through the wireless communication link) allow these waveforms to be addressed to particular LEDs, and therefore particular neural circuits, such that multiple neural circuits may be modulated independently within the same animal. One motherboard module can be used with many differently designed optics modules (e.g. with different numbers of LEDs, different neural targets, etc); indeed, a key aspect of our design is the independence of the modules and the resulting economies of scale for typical academic or industrial neuroscience labs.

Because wireless power by its very nature will vary in efficiency over time (e.g. with the distance between transmitter and receiver), we ensure safe, robust operation of the device using both passive and active/algorithmic strategies. The power module's resonant LC tank circuit is tuned to generate open circuit voltages that, when rectified using a full wave rectifier topology, are below the maximum safe operating voltage of a supercapacitor energy storage element (~ 5.5 V). Nevertheless, to ensure device integrity, we have implemented further safety elements to limit device operation to safe voltage ranges. To maintain a supercapacitor voltage that is within the safety tolerances of the device (that is, below the breakdown voltage of the supercapacitor), an adaptive control loop running on the microcontroller monitors supercapacitor voltage and regulates a switch placed between the rectifier and supercapacitor, limiting current delivered to the supercapacitor as appropriate (e.g. when the LEDs are not operated). The headborne supercapacitor is further protected using a Zener shunt circuit, which acts to short current from the positive terminal of the power rectifier output to the analog power ground terminal, when voltage levels approach the capacitor's 5.5 V rating. It should be noted explicitly that this analog power ground is isolated from the animal, such that no current is dissipated through the animal; in addition, the entire device is physically electrically insulated from the animal (as noted in the methods above). Finally, to maintain safe operating temperatures near tissue, the temperature of the optics module containing the LEDs is continuously monitored using a thermistor mounted on the underside optics module heat sink and a control loop running on the microcontroller. LED operation is disabled once a set temperature is reached, settable

by the user in software, and the device prompts the user via wireless telemetry that a temperature fault has occurred. In our experiments, we limited the allowable operation temperature to within 1 °C of baseline body temperature. We additionally verified that this control circuit was operating at expected temperatures in a bench test setup utilizing a calibrated thermocouple and data logger. Maximum temperature rise in steady state was observed to be approximately 0.6 °C (for a plot of this thermal performance, see supplementary figure 5 available at stacks.iop.org/JNE/8/046021/mmedia). It should be noted that this setup, in which the optics module is not surgically affixed to skull but freely exposed to air, represents a conservative worst-case scenario of heat transfer efficiency, as the total heat capacity of the headborne device is effectively increased when affixed to the animal skull [16, 17].

3.2. How to use the system

Once the headborne device has been assembled as described in section 2 and the optics module is surgically affixed to the skull as described in section 2.2.1 (with coordinates of LEDs chosen based on intended brain targets), the animal is allowed to recover from surgery. With the headborne device attached to the optics module, the animal is able to freely move and behave (figure 1(f)). Once placed in the behavioral arena, the power module automatically activates and begins to charge the onboard supercapacitor, which in turn enables the motherboard and radio modules to self-initialize. The headborne system initiates network pairing with a nearby USB-connected base station if available, and then awaits the instruction of the experimenter. From the base station connected computer, the experimenter may use any serial communication program (e.g. a MATLAB program, custom script, etc) that uses the USB device as a COM port to update the LED activation patterns on each headborne device within range.

Figure 2(c) provides guidelines for usage of wireless headborne optical control devices for typical neuroscience experiments involving pulse trains of light delivery. Here we define terminology for various properties of the pulse train (i.e. within-train duty cycle = $PW/(1/PR)$, and within-train average power = $A * PW * PR$, where A = LED power amplitude, PW = pulse width and PR = pulse rate), for assistance with visualizing typical protocols for device operation. Figure 2(c)(i) graphically shows the range of typical protocols for device operation, expressed as a function of within-train duty cycle and within-train average power, assuming that the between-train pause (i.e. $ITI - 2 * TD$, where ITI = inter-train interval, TD = train duration) is at least 3 s (a simplifying assumption that would be compatible with many neuroscience experiments—this assumption allows us to assume that the supercapacitor always has time to recharge between trains; by taking into account partial charging, the potential for other protocols can be estimated). Any point under the purple curve is easily achievable. Because the power antenna continuously receives 2 W, the device can run indefinitely with a time-averaged power of 2 W; the device can exceed 2 W using the supercapacitor's excess capacity, but with reduced duty cycle, and never crossing

the device maximum peak power of 4.3 W (higher maximum peak powers are easily achievable with use of higher capacity supercapacitors; we chose a 400 mF capacitor in this instantiation based on expected current draw for motor control applications). At 4.3 W, these performance figures translate to four 1 mm × 1 mm LEDs being driven at 50% duty cycle for 3 s with 3 s ITI, or eight of the same LEDs for 1.5 s bursts at 50% duty cycle, or 16 LEDs for 0.75 s bursts at 50% duty cycle. In continuous operation, 2 of these LEDs can be driven at 100% duty cycle to consume 2 W. There is no hit in device performance with between-train pauses of less than 3 s if 2 W or less is consumed; if more than 2 W is consumed, because the supercapacitor's excess capacity is needed, some time (up to 3 s, depending on how much energy is used) will be required to recharge the supercapacitor in between the LED-on periods that drain the supercapacitor during the pulse train delivery.

The total energy is stored on the supercapacitor scales as the square of the voltage on the capacitor. The LED forward voltage is typically ~3.6 V, well within the range of the 5.5 V maximum voltage allowed on the supercapacitor used in this design. To make the stored energy on the supercapacitor available for LED operation during periods in which supercapacitor voltage transiently drops below this 3.6 V (e.g. high current pulsatile trains, changes in head distance from the transmitter), a two-stage power conversion scheme is implemented to boost circuit output voltage. In this manner, nearly the full operating voltage range of the supercapacitor (and therefore, nearly the full range of energy stored) may be utilized for LED power by utilizing a combination of a first stage boost converter circuit topology, which up converts voltage on the supercapacitor from as little as 0.3 V to the LED's typical 3.6 V forward voltage, as well as a second stage of switched capacitor LED drivers which provides current regulation.

3.3. Demonstration of remote motor control

We demonstrate the applicability of this technology to untethered freely-behaving animal optogenetics, using a well-validated and easily-quantified behavioral paradigm of cortically-driven unilateral motor control in the mouse [6]. A simple paradigm in which 470 nm light was delivered unilaterally to M1 motor cortex at 30 Hz with 15 ms pulse width at 250 mW LED input power in 30 s epochs followed by 90 s periods of rest resulted in increased rotation to the contralateral side during stimulation as compared to the epoch before stimulation (figure 2(d), right, $p < 0.01$, paired t -test, $n = 9$ trials in two animals). Thus, we can drive behaviorally-relevant protocols at sufficiently high power levels to elicit robust behavioral changes.

We measured the magnetic field produced by the power transmitter and found that peak field strength was less than 300 A m⁻¹, orders of magnitude less than that shown to affect neural excitability or drive neural activity [18]. We additionally performed a direct control experiment, repeating the motor control experiment with just the LED outputs disabled (i.e. by disabling the LED controller (shown in figure 1(a)) via program pins). In this control experiment,

the animal experiences the electromagnetic field, power and control signals are received by the headborne device, and the power receiver dissipates heat via shunting of received current in the supercapacitor control circuit, but no light is emitted from the LED. We observed no change in rotational behavior in this experiment (figure 2(d), left, $p > 0.50$, $n = 5$ trials in one subject). As mentioned above, we further control for temperature-related effects by limiting the maximum rise in optics module temperature to less than 1 °C, itself insulated from the brain by high thermal resistivity epoxy and skull.

4. Discussion

The system described here expands upon existing tethered behaving animal optogenetic strategies, by enabling truly wireless freely-behaving optogenetics. The device described here is able to operate indefinitely while delivering up to 2 W of power to an array of LEDs from a compact under-cage or under-behavioral-arena power transmitter operating at low-strength magnetic fields (300 A m⁻¹), and is able to deliver up to 4.3 W of power intermittently by utilizing a supercapacitor-based energy storage system to buffer the wireless power link. This system provides the ability to control many headborne devices simultaneously using software polling techniques that are amenable to high-throughput *in vivo* neural circuit screening. Without the requirement to physically connect and disconnect each animal as in previous tethered approaches, this untethered system further reduces potential behavioral artifacts associated with animal handling and possible torque on the animal's head from a tethered fiber. Animals in our experiment were observed for at least three months with implanted optics modules, and exhibited natural grooming, nesting and exploratory behavior throughout this time frame, suggesting that this approach does not interfere with normal animal livelihood. We are currently evaluating future iterations of the design presented here, and applying the untethered optical neural control setup to new optogenetic research paradigms, briefly described in the following sections.

4.1. Future directions

The headborne device presented here is sufficiently compact in size to enable use in mouse experiments, at approximately 2 g total weight in pre-programmed operation and less than 3 g with the optional radio module, which enables real-time updating from a PC. The supercapacitor-based storage element enables up to 4.3 W of intermittent power delivery, directable to up to 16 LEDs. In future implementations, it would be feasible to target deep brain structures with this design by attaching optical fibers to the surface of the LEDs. Several under-cage power transmitters may also be tiled to cover large area mazes or other environments, enabling a new class of optogenetic research paradigms.

Nearly all of the underlying technologies enabling this device (system-on-chip telemetry and microcontroller systems, solid state light sources, wireless power transfer, thin film supercapacitors) are being improved daily, driven by their applications to this and other fields such as computing,

telecommunications, and energy. Thus, we expect the performance of this system to be further improved as individual technologies mature. The use of solid state miniature lasers in particular would enable a substantial reduction in the net power requirements of the system (LEDs are an uncollimated light source with Lambertian distribution, and thus the light spread is broad). Alternatively or in addition, development of light-sensitive ion channels compatible with existing solid state laser technology, e.g. with activation spectra shifted to the red wavelengths, would substantially increase the power efficiency of this system overall. In energy storage, development of higher energy density supercapacitors or hybrid supercapacitor + rechargeable battery systems will improve the performance of this system over longer timescales, such that wireless charging requirements may be relaxed. The use of far-field wireless power delivery techniques may further simplify the delivery of charging power. By riding technology development curves, the system described here may eventually be miniaturized to a few mm², further increasing its applicability to research and potentially enabling clinical applications not addressable with today's devices.

Clinically, modulation of neural circuits via electrical stimulation (deep brain stimulation, or DBS) has been demonstrated successfully in the treatment of Parkinson's disease and dystonia symptoms, with several other promising indications in clinical trial. These DBS approaches to treating neurological disorders rely on an implanted pacemaker-like device, implanted either in the chest [19] or cranium [20], itself composed primarily of a large battery, providing power to current sources, which in turn deliver therapeutic stimulation to several electrode contacts by way of a flexible single lead or pair of leads. While this approach has proven highly efficacious for the neurological disorders mentioned above (among others), side effects are often reported with this modality and are believed to originate from the unwanted recruitment of nearby neuronal cell bodies and axons [21]. The single-cell-type specificity enabled by optogenetic implementations may therefore be a potential avenue to pursue to eliminate the side effects observed with existing electrical DBS approaches.

Finally, substantial risk of clinical device failure has been attributed to breakage of the flexible leads connecting the large implantable pulse generator and the implanted electrodes [22]. As the number of target sites of therapeutic interest increases, particularly as DBS technologies are deployed in diseases where the pathology cannot be traced to a single, statically defined brain region (e.g. epilepsy), the issue of delivering therapeutic stimulation to the target site without risk to the patient will become increasingly difficult. One can therefore envision a system in which this lead is replaced by a wireless power link, and the electrode is replaced by a miniaturized version of the headborne system described here, such that many brain regions may be independently addressed therapeutically, each receiving power and control signals wirelessly from a small implantable antenna on the surface of the brain. Using such an approach, it may be possible to develop truly adaptable, brain-wide DBS-like therapies to target disorders intractable to current pharmacological or device-based therapies.

Acknowledgments

ESB acknowledges funding by the NIH Director's New Innovator Award (DP2OD002002) as well as NIH Grants 1R01DA029639, 1RC1MH088182, 1RC2DE020919, 1R01NS067199 and 1R43NS070453; the NSF CAREER award, as well as NSF Grants EFRI 0835878, DMS 0848804 and DMS 1042134; Benesse Foundation, Jerry and Marge Burnett, Department of Defense CDMRP PTSD Program, Google, Harvard/MIT Joint Grants Program in Basic Neuroscience, Human Frontiers Science Program, MIT McGovern Institute and the McGovern Institute Neurotechnology Award Program, MIT Media Lab, MIT Mind-Machine Project, MIT Neurotechnology Fund, NARSAD, Paul Allen Distinguished Investigator in Neuroscience Program, Alfred P Sloan Foundation, SFN Research Award for Innovation in Neuroscience and the Wallace H Coulter Foundation. CTW designed, fabricated and tested the wireless system and contributed to the manuscript, with technical support for power transmitter implementation from Ferro Solutions, which provided the wireless transmitter. JGB designed the core of the optics module and fabricated these components with assistance from AG. PM performed animal surgeries and assisted in behavioral experiments, with assistance from AR. ESB provided many insights into system and experiment design and invaluable contributions to the manuscript. The authors thank X Han for her assistance with behavioral experiments.

References

- [1] Boyden E S *et al* 2005 Millisecond-timescale, genetically targeted optical control of neural activity *Nat. Neurosci.* **8** 1263–8
- [2] Han X and Boyden E S 2007 Multiple-color optical activation, silencing, and desynchronization of neural activity, with single-spike temporal resolution *PLoS ONE* **2** e299
- [3] Zhang F *et al* 2007 Multimodal fast optical interrogation of neural circuitry *Nature* **446** 633–9
- [4] Chow B Y *et al* 2010 High-performance genetically targetable optical neural silencing by light-driven proton pumps *Nature* **463** 98–102
- [5] Gradinaru V *et al* 2010 Molecular and cellular approaches for diversifying and extending optogenetics *Cell* **141** 154–65
- [6] Aravanis A M *et al* 2007 An optical neural interface: *in vivo* control of rodent motor cortex with integrated fiberoptic and optogenetic technology *J. Neural Eng.* **4** S143
- [7] Bernstein J G *et al* 2008 Prosthetic systems for therapeutic optical activation and silencing of genetically-targeted neurons *Proc. Soc. Photo-Opt. Instrum. Eng.* **6854** 68540H
- [8] Huber D *et al* 2008 Sparse optical microstimulation in barrel cortex drives learned behaviour in freely moving mice *Nature* **451** 61–4
- [9] Arfin S K *et al* 2009 Wireless neural stimulation in freely behaving small animals *J. Neurophysiol.* **102** 598–605
- [10] Iwai Y *et al* 2011 A simple head-mountable LED device for chronic stimulation of optogenetic molecules in freely moving mice *Neurosci. Res.* **70** 124–7
- [11] O'Handley R C, Huang J K, Bono D C and Simon J 2008 Improved wireless, transcutaneous power transmission for *in vivo* applications *IEEE Sensors J.* **8** 57–62
- [12] Arenkiel B R *et al* 2007 *In vivo* light-induced activation of neural circuitry in transgenic mice expressing channelrhodopsin-2 *Neuron* **54** 205–18
- [13] Wang H *et al* 2007 High-speed mapping of synaptic connectivity using photostimulation in Channelrhodopsin-2 transgenic mice *Proc. Natl Acad. Sci. USA* **104** 8143–8
- [14] Parallikar K, Cong P, Santa W, Dinsmoor D, Hocken B, Munns G, Giftakis J and Denison T 2010 An implantable 5 mW/channel dual-wavelength optogenetic stimulator for therapeutic neuromodulation research *IEEE Solid State Circuits Conference Digest of Technical Papers (ISSCC) 2010 (San Diego, CA)* pp 238–9
- [15] Sarpeshkar R 2010 *Ultra-Low Power Bioelectronics* (Cambridge: Cambridge University Press)
- [16] Janssen F E, Van Leeuwen G M and Van Steenhoven A A 2005 Modelling of temperature and perfusion during scalp cooling *Phys. Med. Biol.* **50** 4065–73
- [17] Kassakian J G, Schlecht M F and Verghese G C 1991 *Principles of Power Electronics* (New York: Addison-Wesley)
- [18] Radman T *et al* 2009 Role of cortical cell type and morphology in subthreshold and suprathreshold uniform electric field stimulation *in vitro Brain Stimulation* **2** 215–28
- [19] Caparros-Lefebvre D *et al* 1993 Chronic thalamic stimulation improves tremor and levodopa induced dyskinesias in Parkinson's disease *J. Neurol. Neurosurg. Psychiatry* **56** 268–73
- [20] Skarpaas T L and Morrell M J 2009 Intracranial stimulation therapy for epilepsy *Neurotherapeutics* **6** 238–43
- [21] Schuurman P R *et al* 2000 A comparison of continuous thalamic stimulation and thalamotomy for suppression of severe tremor *N. Engl. J. Med.* **342** 461–8
- [22] Oh M Y *et al* 2002 Long-term hardware-related complications of deep brain stimulation *Neurosurgery* **50** 1268–74 1274–6 discussion

Supplementary Files –

1. Supplementary Table 1: Experiment Statistics

	LED driver active (experimental condition)				LED driver disabled (control condition)	
	Animal # 658		Animal # 2483		Animal # 2483	
Trial #	Pre- stimulus*	Stimulus*	Pre-stimulus	Stimulus	Pre- stimulus*	Stimulus*
1	0.5	2.25	0.25	1.5	.25	.25
2	0.0	1.5	0	1.75	.5	.25
3	0.5	1.75	-0.5	1.5	0	0
4	0.5	1.5	0.25	1.5	.25	.5
5	0.25	1.5			.25	0
Mean	0.35	1.70	0	1.75	.25	.2
Std. Dev.	0.22	0.33	0.35	0.13	.088	.10
Student's T-test	P = 0.0004		P = 0.0036		P = .6213	
Student's T-test, combined data	P = 0.00000024					

*indicates animal rotations per 30 second interval (positive is counter-clockwise direction)

2. Circuit Schematics – High Resolution PDF schematics follow this document.

Supplementary Figure 1: Motherboard Module

Supplementary Figure 2: Optics Module – Single Bank Control Logic

Supplementary Figure 3: Radio Module

3. Use of Software

Opening an experiment session. The experimenter can initialize the wireless network by plugging the USB interfaced wireless base station into a PC running Windows XP or Vista (For Mac users, functionality has been also verified using a Windows XP virtual machine session using VMware Fusion in OS X v10.4 and higher) and opening a Hyperterminal session with the tether. The base station appears as a COM port on the PC; the specific port address (e.g. COM3) will vary from machine to machine, but may be found by navigating to the Device Manager and expanding the “Ports (COM & LPT)” tab (in Windows XP, Control Panel -> System -> Hardware -> Device Manager). When recognized by the computer, the base station will appear as “MSP430 Application UART.” With the COM port identified, the Hyperterminal session may be opened (using 9600 baud, 8-N-1, and no parity bit UART port control settings). These parameters can be saved as a pre-configured Hyperterminal session to ease future setup.

Running the Experiment. Once the Hyperterminal session is opened, the user is greeted with a splash screen outlining all of the software commands supported by the wireless system. This user interface is hosted on the base station to simplify the software needs. A simple experiment session with a remotely triggered 130 Hz, 5ms pulse train on LED1 is described below.

Typing, “Hello” will list all of the networked wireless devices in the range of the base station. All network pairing is handled behind the scenes to simplify operation. Each device is identified by a unique 4-digit hexadecimal ID tag (e.g., “CAFE”), which was assigned to the device when it was programmed and may be customized to suit the documentation protocol of the laboratory. To address a specific device, the command must be preceded by the device name (see example below).

We first select the desired output channel. “ST=1” will set the output channel to LED 1. We next set the pulse width and frequency of the selected channel. “PW=x” will set the pulse width of stimulation to x milliseconds. “FR=x” sets the pulse frequency to x Hz. With these parameters sent, the stimulation engine on the remote device is now set, and the device can be toggled on/off with user commands (“GO” and “STOP”). The device is now in active transmit/receive mode, so the latency between the user’s requesting a pulse train and the start of the train on the remote device is <1ms.

Sample Hyperterminal Session:

=> Hello

“Networked Devices Found: CAFE”

=> CAFE ST=1

“Device CAFE channel 1 initialized”

=> CAFE 1 PW=5

“Device CAFE channel 1 pulse width set to 5 ms”

=> CAFE 1 FR=130

“Device CAFE channel 1 frequency set to 130 Hz”

=> CAFE 1 GO

“Device CAFE channel 1 active”

=> CAFE 1 STOP

“Device CAFE channel 1 stopped”

Remote Device Control: User Commands

Hello – returns the IDs of all networked headborne devices.

ST – selects the LED channel to be programmed (must be preceded by device ID)

PW – sets the pulse width in milliseconds of the stimulation waveform (preceded by ID and channel)

FR – sets the frequency of the stimulation waveform in Hz (preceded by ID and channel)

GO – toggles stimulation waveform on (must be preceded by device ID and channel number, e.g. “CAFE 1 GO”)

STOP – toggles stimulation waveform off (must be preceded by device ID and channel number, e.g. “CAFE 1 STOP”)

SLEEP – sends the target device into idle mode for a period of time, in seconds. Note that this command will result in shutdown of the radio chipset! Upon elapse of the sleep period, the device will wake up, initialize the radio and reconnect to the network. (must be preceded by device ID)

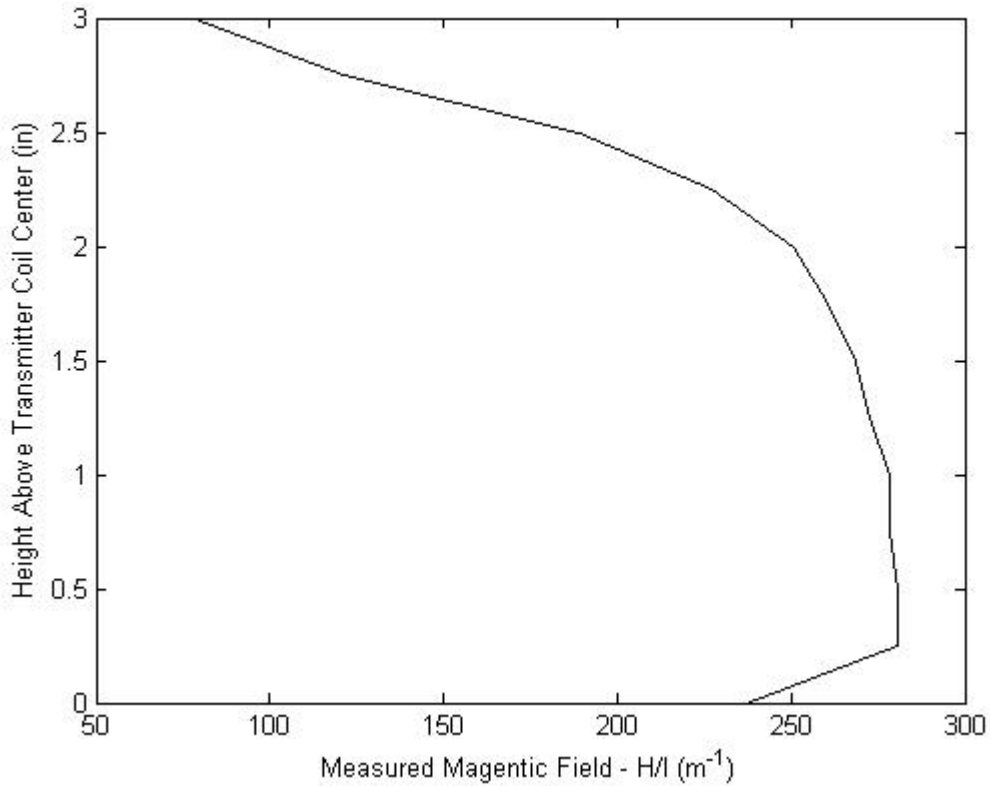
MATLAB scripting of experiment sessions: If precise temporal control of waveform toggle, generation of complex waveforms, or automated experiment sessions for high-throughput use is desired, a control script can be implemented in MATLAB (Mathworks) or any number of alternative open source languages featuring I/O port control, (e.g. Python). For detailed descriptions and modifications required to support Mac or Linux operation, see the Mathworks support page, [here](#).

All commands described above are interpreted by the USB base station identically, whether through Hyperterminal or any other COM port interface. One simply initializes the COM port according to the command below, and then may proceed as described above using the wireless system's native command set. Pre-written m-files can then run autonomous experiment sessions of substantial complexity.

```
port = serial ('com1', 'BaudRate', 9600, 'Parity', 'none', 'DataBits', 8, 'StopBits', 1);
```

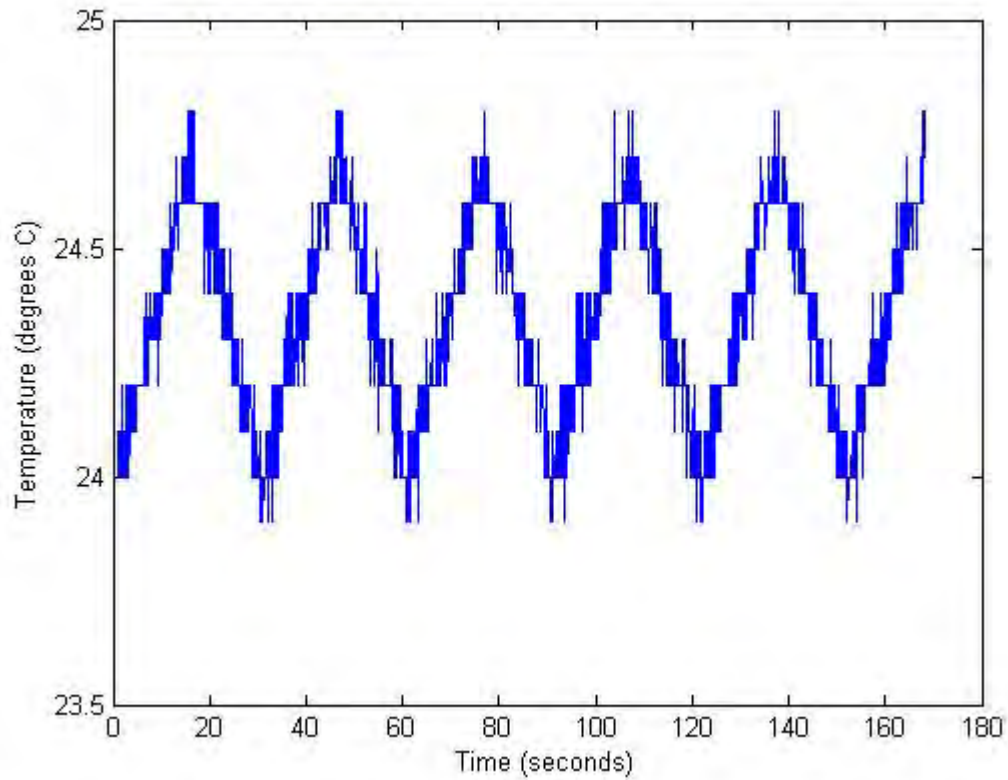
Note: Be sure to set 'com1' to the appropriate port name.

4. Measurement of power transmitter's magnetic field strength



Supplementary Figure 4: Power Transmitter Magnetic Field Strength. Magnetic Field M produced by power transmitter coil per Ampere's law is measured about the vertical axis (coming out of the power transmitter coil, perpendicular to the cage floor), as described in Methods and field strength is plotted as a function of distance above the power transmitter coil. Note the convention of unit H/I, where I=5A is the DC current inside the transmit coil.

5. Measurement of Optics Module – Skull Interface Temperature Under LED Operation



Supplementary Figure 5: Optics module steady-state operating temperature. Temperature of optics module thermal sink (LED-side) was measured as described in Methods. Supp. Fig. 5 shows steady state thermal profile of the optics modules used in actual behavioral experiments, under bench testing with a 15 second on / 15 second off pulse train of 30 Hz, 50% duty cycle operation using a lightweight 1 gram heat sink.

